Chemical Science

ROYAL SOCIETY OF CHEMISTRY

EDGE ARTICLE

View Article Online
View Journal | View Issue

Cite this: *Chem. Sci.*, 2024, **15**, 8062

All publication charges for this article have been paid for by the Royal Society of Chemistry

Crucial gating residues govern the enhancement of peroxygenase activity in an engineered cytochrome P450 *O*-demethylase†

Panxia Zhao,‡[ac] Yiping Jiang,‡[abd] Qian Wang,‡[a] Jie Chen,[abd] Fuquan Yao[a] and Zhiqi Cong *[abcd]

Received 12th April 2024
Accepted 2nd May 2024

DOI: 10.1039/d4sc02418d

rsc.li/chemical-science

P450-catalyzed *O*-demethylation reactions have recently attracted particular attention because of their potential applications in lignin bioconversion. We recently enabled the peroxygenase activity of CYP199A4, a NADH-dependent cytochrome P450 monooxygenase from *Rhodopseudomonas palustris*, by engineering a hydrogen peroxide (H_2O_2) tunnel. In this report, we reveal by crystallography and molecule dynamics simulations that key residues located at one of the water tunnels in CYP199A4 play a crucial gating role, which enhances the peroxygenase activity by regulating the inflow of H_2O_2. These results provide a more complete understanding of the mechanism by which monooxygenase is converted into peroxygenase activity through the H_2O_2 tunnel engineering (HTE) strategy. Furthermore, a library of engineered CYP199A4 peroxygenases was constructed to explore their application potentials for *O*-demethylation of various methoxy-substituted benzoic acid derivatives. The engineered CYP199A4 peroxygenases showed good functional group tolerance and preferential *O*-demethylation at the *meta*- or *para*-position, indicating potential *O*-demethylation of H- and G-type lignin monomers. This work reveals the feasibility of the HTE strategy in creating P450 peroxygenase from a mechanistic perspective, laying the foundation for developing an effective P450 *O*-demethylase applicable in lignin bioconversion.

Introduction

Lignin is an abundant renewable resource in nature that is composed of three phenylpropanol units, *p*-coumaryl guaiacol (H), coniferyl alcohol (G) and sinapyl alcohol (S).[1] One approach that has the potential to overcome the lignin utilisation barrier is biological funnelling, which utilises microbial pathways to convert heterogeneous chemical mixtures into a defined product with high atomic efficiency, especially suitable for aerobic decomposition of aromatic compounds.[2] In bacteria, aromatic compounds can be degraded to lignin derivatives (LDACs). LDACs such as 4-methoxybenzoic acid, guaiacol, valerianol and eugenol have one or two methoxy groups on their aromatic rings.[3] *O*-demethylation to diols or phenolic hydroxyls is a key step for converting lignin-derived monomer compounds into high-value-added bioproducts, and these reactions are mainly carried out by microorganisms such as white, soft and brown rot fungi and some bacteria.[3–5] Although several *O*-demethylases of lignin and its derivatives have been identified in aromatic catabolism for microbial lignin conversion, the use of these oxidizing enzymes still suffers from narrow substrate specificity, unclear reaction mechanisms and lack of reductase partners.[6,7] Thus, interest in mining for novel demethylation enzyme genes or engineering demethylation isoenzymes to yield practical demethylase catalysts has increased.

In recent years, cytochrome P450 (CYP or P450), a heme-dependent enzyme that is a versatile bio-oxidation catalyst for C–X (*e.g.*, X = H, N, S) bond oxidations,[8] has revived interest in the *O*-demethylation of lignin monomer derivatives. For example, the two-component P450 enzyme GcoAB from the CYP255A subfamily and its variants efficiently catalyze the demethylation of guaiacol and syringol,[6,9] whereas CYP199A4 from *Rhodopseudomonas palustris* catalyzes the demethylation of G-type lignin monoaromatics.[10] In addition, considering that these enzymes require the expensive cofactor NAD(P)H and complex electron transfer chains to support the activation of molecular oxygen, scientists have also been especially interested in P450 peroxygenase driven by economical and environmentally friendly hydrogen peroxide (H_2O_2).[11–13] Some engineered P450 peroxygenase systems and characterised new cytochrome P450 *O*-demethylase have been reported for the *O*-demethylation of lignin monomer analogs.[14–17]

[a]*CAS Key Laboratory of Biofuels, Shandong Provincial Key Laboratory of Synthetic Biology Qingdao Institute of Bioenergy and Bioprocess Technology, Chinese Academy of Sciences Qingdao, Shandong, P. R. China. E-mail: congzq@qibebt.ac.cn*
[b]*Shandong Energy Institute, Qingdao, Shandong, 266101, China*
[c]*University of Chinese Academy of Sciences (UCAS), Beijing 100049, P. R. China*
[d]*Qingdao New Energy Shandong Laboratory Qingdao, Shandong, P. R. China*

† Electronic supplementary information (ESI) available. See DOI: https://doi.org/10.1039/d4sc02418d

‡ These authors contributed equally.

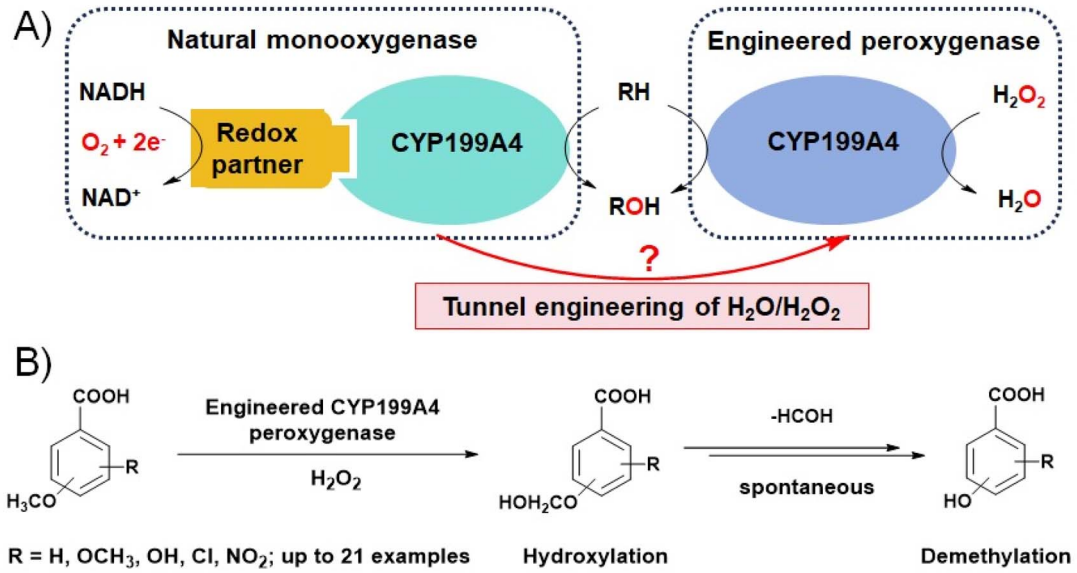

Scheme 1 (A) Tunnel engineering strategy of H_2O/H_2O_2 to transform natural P450 monooxygenase to engineered P450 peroxygenase. (B) Catalytic *O*-demethylation of methoxy-substitute benzoic acid derivatives by engineered CYP199A4 peroxygenase.

Very recently, we reported the rational conversation of NAD(P)H-dependent P450 monooxygenases to their peroxygenases modes by engineering their intrinsic water tunnels to favor the inflow of H_2O_2 into the active site (heme center), the so-called H_2O_2 tunnel engineering (HTE) strategy.[18] The strategy has been employed efficiently for generating or improving CYP199A4, CYP153A$_{M.aq}$ and DFSM-facilitated P450BM3 peroxygenases; however, the mechanism of how H_2O_2 enters the active site of P450 enzymes remains unclear.

Given its significant potential for creating P450 peroxygenases from monooxygenases, in this report, we scrutinized the molecular mechanism of peroxygenase activity in CYP199A4 initiated through the HTE strategy by combining X-ray crystallography and molecular dynamics (MD) simulations to elucidate the crucial role of gating residues. Furthermore, we demonstrate the potential application of the engineered CYP199A4 peroxygenase variant in the *O*-demethylation of various electron-donating or electron-withdrawing (methoxy, nitro, hydroxy and methyl) substituted benzoic acid derivatives, including typical H- and G-type lignin monoaromatic hydrocarbon analogs (Scheme 1).

Results and discussion

Structural insights into the H_2O_2 tunnel engineering strategy

The F182A mutant not only exhibited the highest activity among all single mutants but also served as the parent enzyme for double mutants. Therefore, the CYP199A4 F182A mutant in complex with 4-methoxybenzoic acid (4-MBA) was co-crystallized, and the structure was determined at 1.53 Å resolution. The electron densities of heme, 4-MBA, key residues (A182 and D251) and surrounding water molecules were of sufficient quality to analyze the binding mode of the ligand (Fig. 1A). The structure clearly shows a potential H_2O tunnel nearly separated into two segments by the residue pair of F182A and D251. Five water molecules are found above the heme center and inside the A182/D251 pair, whereas four and zero water molecules are observed in the same regions of the F182T and wild-type (WT) enzymes, respectively (Fig. 1B). In contrast, numerous water molecules are found outside residues D251 and F182 in all three structures. This observation suggests that the residue pair of F182 and D251 plays a possible gating role in H_2O inflow. Considering the very similar physicochemical properties of H_2O_2 and H_2O [*e.g.*, molecular diameter (0.25–0.28 nm *vs. ca.* 0.275 nm), dipole moment (2.26×10^{-18} esu *vs.* 1.85×10^{-18} esu) and dielectric constants (73.1 *vs.* 80.4 [H_2O])[20,21] indicates that a smaller-sized residue at position 182 should facilitate the inflow of H_2O_2 molecules into the active center. This postulate may well explain the catalytic capacities of the H_2O_2-dependent demethylation of 4-MBA by mutants F182A and F182T and WT CYP199A4, which gave catalytic turnover numbers (TONs) of 980, 103 and 6 μM (μM P450)$^{-1}$, respectively.[18] These results establish a possible proportional relationship between the amount of H_2O_2 entering and catalytic activity. In comparison to F182T, the presence of a smaller alanine side chain in F182A enables an additional water molecule (w5) to access the active center. This influx of w5 not only enhances the local polarity but also results in a redistribution of hydrogen bond networks. Consequently, this rearrangement facilitates the methoxy group of 4-MBA to flip towards the heme. This orientation of the methoxy group was much closer to the iron center and w1, which further promoted the demethylation reaction and could be a reasonable explanation for the higher activity observed in F182A. Although the orientation of the methoxy group of 4-MBA in WT was similar to that of F182A and favored for demethylation, the inaccessibility to H_2O_2 severely diminished its peroxygenase activity. Therefore, both the entrance of H_2O_2 and the orientation of substrate were the key

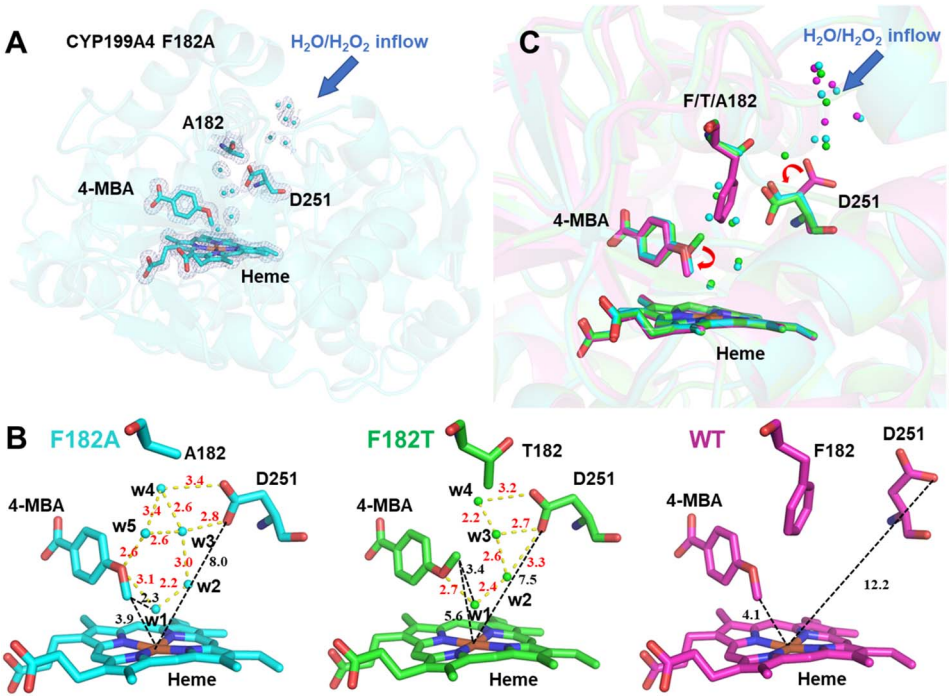

Fig. 1 Structural insights into the improved peroxygenase activity after mutagenesis at the key gating residue F182. 4-Methoxybenzoic acid, heme and gating residues are represented as stick models, and water molecules are drawn as spheres. (A) CYP199A4 F182A crystal structure in complex with 4-MBA (PDB ID: 8WS4). The 2Fo-Fc electron density maps contoured at 1.0σ are shown as a light gray mesh. (B) Active sites of F182A (cyan), F182T (PDB ID: 8HGC, green) and wild type CYP199A4 (PDB ID: 4DO1,[19] magenta) in complex with 4-MBA. Hydrogen bonds are shown as yellow dashed lines and their distances are noted in red. The distances among the methoxyl group of the substrate, distal coordinated water molecule w1, D251 and heme iron are labeled as a black dashed line in each structure. (C) Structural superposition of WT CYP199A4 (magenta), F182T (green) and F182A (cyan).

factors for the demethylation reaction, while the former had a greater impact. In addition, the side chain of D251 was flipped toward the active site in the structures of F182A and F182T, probably serving as the H_2O-mediated catalytic base for H_2O_2 activation, as supported by the following stability test and the theory proposed previously.[18,22,23] In contrast, the observed low peroxygenase activity of WT enzyme exemplifies its absence of a defined activation mechanism for the activation of H_2O_2. Notably, all the ligands, residues and waters showed in Fig. 2 had occupancies of 1.0, expect for w1 of F182A with an occupancy of 0.8, consisting with their spectra change when adding the substrate (Fig. 2). For WT, 4-MBA expelled the distal coordinated water molecule as expected, leading to Soret band shifted to 395 nm. However, only a small proportion of high-spin state enzyme was observed upon the addition of 4-MBA for F182A, while w1 in F182T still coordinated with the heme iron since minimum high-spin shift was identified.

Next, to further validate the stability of CYP199A4, we examined the kinetics of heme degradation in WT, F182A, F182T, F182A/D251N and F182A/D251E. In the presence of 10 mM and 2 mM 4-MBA, the degradation rate of WT was 3.6×10^{-4}, which was higher than that of F182A/D251N (2.7×10^{-4}) and F182A/D251E (1.9×10^{-4}), but F182A (1.0×10^{-3}) and F182T ($3.\ 8 \times 10^{-3}$) were more than 10-fold faster, suggesting that H_2O_2 was able to enter the active pockets of F182A and F182T and generate active species compound **I**, most of which were used in the demethylation reaction (Fig. S2†). We also observed a TON of up to 1900 for the longer demethylation reaction of 4-MBA at 30 °C after 5 h. The above results indicate the relative stability of the F182A mutant (Fig. S3†).

Molecular dynamic (MD) simulations

We performed MD simulations to further understand the increased peroxygenase activity of the F182 mutations. The enzyme and substrate were fully solubilized with H_2O (containing more than 20 000 H_2O molecules). All H_2Os within 10 Å of the heme were removed to ensure no H_2O was within the active site in the initial conformation. Classical MD simulations were used for an undifferentiated examination of all possible water tunnels in the enzyme structure. The best single mutation, F182A, was first chosen to perform a simulation for 500 ns. Three H_2Os eventually appear in the active site, two passing between A182 and D251 into the active site after remaining near D251 for 100 ns and 2 ns, respectively (Fig. 3A and B). This result shows that the tunnel between A182 and D251 exists, and the potential energy barrier is probably low. The third H_2O entered the site above the middle position between T252 and the substrate (Fig. S4C†). We hypothesize that the attraction of D251 initiates the crossing process. Compared with no stopping at all, stopping near the entrance of the tunnel can increase the probability that the H_2O overcomes the potential barrier. Based on the parent F182A enzyme, we mutated D251 to A, G, N, H and

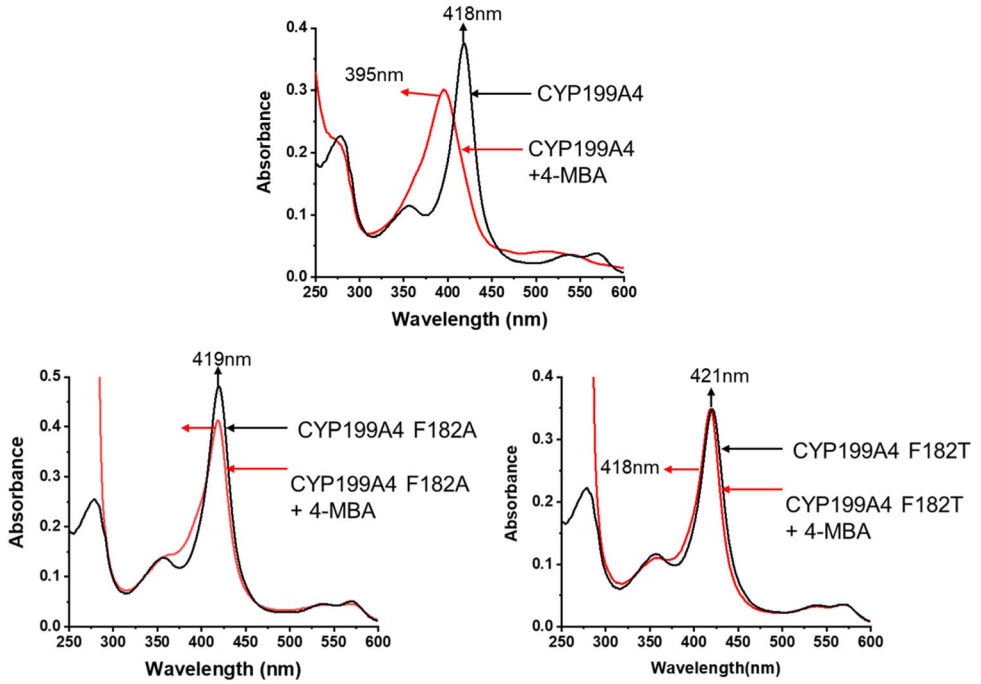

Fig. 2 Spin state shift spectroscopy of CYP199A4, F182A and F182T induced by 4-methoxybenzoic acid (4-MBA).

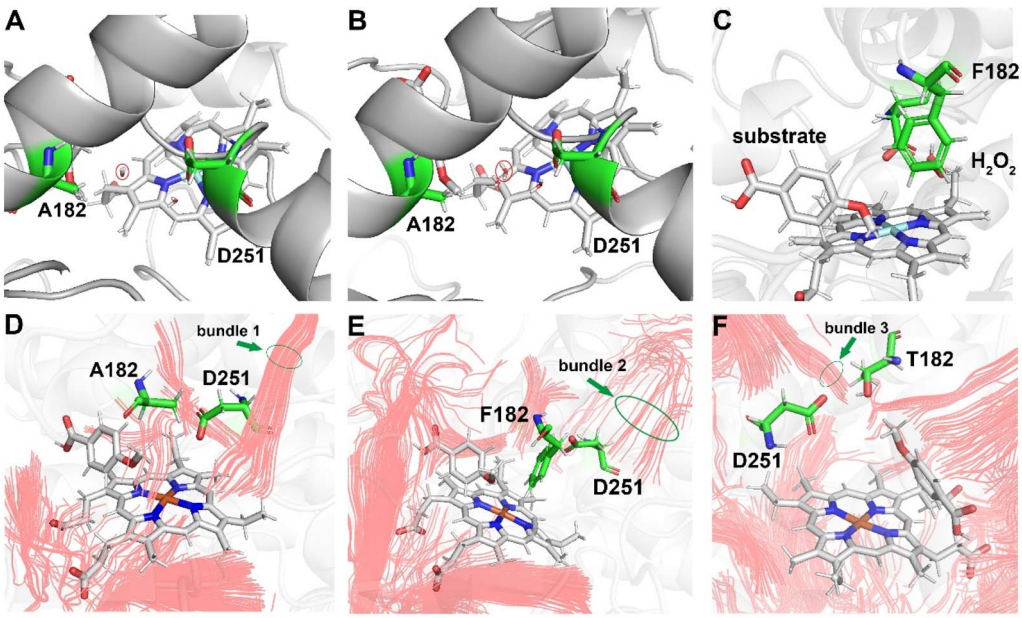

Fig. 3 (A and B) H_2O molecules passing through the water tunnel of F182A in 500 ns. (C) Conformational changes to the F182 side chain and substrate when H_2O_2 passes through the wild-type tunnel. (D–F) Streamlines of water in F182A, wild-type and F182T, respectively.

E to verify the important role of D251. As a result, the catalytic activities of F182A/D251N, F182A/D251H and F182A/D251E toward 4-MBA were reduced 50-fold compared with that of F182A, whereas F182A/D251A and F182A/D251G lost catalytic activity completely (Table S2†). These results support our hypothesis that mutation of D251 alters the surrounding H-bond network, which affects the activation of H_2O_2.

Similar 500 ns MD simulations of the WT, largely inactive mutants F182A/D251E and F182A/D251A further validated the above claims. In the WT simulation, one H_2O crosses the tunnel by interacting with the inner side of D251 so rapidly that the long side chain of F182 has no effect on it (Fig. S4A†). This shows that the potential energy barrier of this tunnel may be so large that H_2O can only pass through occasionally. In F182A/

D251E, although E251 similarly attracts some H_2Os, no H_2O entered the tunnel. The single H_2O that entered the site traversed through a gap created by three helices in which V159, T253 and A364 are located, respectively (Fig. S4B†). Thus, the longer side chain of E251 likely increased the difficulty for H_2O to escape from electrostatic interactions. In F182A/D251A, although the distance between A182 and A251 is larger than that in the WT protein, the aggregation of H_2O is distal from these residues, which is most likely caused by the absence of electrostatic attraction, so no H_2O entered the tunnel. However, the three H_2Os still entered through other occasional tunnels.

The first enters from a position similar to the third one in the F182A, the second passes through a gap between R125 and A364, and the third H_2O passes from the bottom upwards near the two carboxyl groups of heme to reach the site (Fig. S4D and E†). The passing efficiency of F182A has been significantly improved, likely as a result of the ample width and the attractive forces of D251 towards H_2O. This notion also has been well verified by the results for two other double mutants: neither F182A/D251E, which can also attract but has a longer side chain, nor F182A/D251A, which has a greater width but lacks the attractive forces, allowed H_2O to pass. These statistics and analyses have demonstrated a clear positive correlation between the number of H_2Os entering the site through this tunnel and the enzyme activity. To compensate for possible biases in sampling statistics, we used the streamline analysis algorithm developed by Vassiliev *et al.* to explore water flow trends.[24,25] The algorithm locates areas of highly anisotropic motions of H_2Os by calculating the diffusion tensor fields over the entire simulation, thus finding the most likely pathways of water diffusion in the protein.[26] A streamline analysis was initially performed on F182A, revealing that the protein is covered with streamlines around and inside the protein (Fig. S1I†). This result indicates that the force field formed by the protein gives clear directions to the diffusion of H_2O around it. Moreover, the streamlines inside the protein are much denser than those around the periphery (Fig. S4J†), apparently because of the stronger force field inside. When investigating the streamlines near the active site (Fig. 3D), we found that a very dense bundle of streamlines passes through the tunnel and reaches the bottom of the tunnel (bundle 1), indicating that the mutated tunnel can direct the flow of water to the active site and reach the area near the heme. A bundle of streamlines also forms around the tunnel in WT (Fig. 3E), but it is much more sparse, and comes to a halt at the top of the entrance (cluster 2). This suggested that while the outer residues enable water to flow towards the tunnel, the residues at the entrance hinder this directional diffusion. Because there are also H_2Os present in the tunnel of F182T, the same classical simulation and streamline analysis were performed on F182T for comparison (Fig. 3F). We observed that the streamline density at the tunnel is significantly higher than that of the wild type and closer to F182A (bundle 3). In terms of diffusion depth, although the streamlines did not directly enter the active site as in F182A, they reached a position parallel to T182 and D251, penetrating about 1 Å more than the WT. At this position, the probability of H_2O diffusing freely into the active site is evidently greater than that of diffusion from the entry above, but there is still a fundamental difference compared to the direct flow into the active site as in F182A. Considering the sequential decrease in activity from F182A, F182T, to Wild Type, this conclusion, which provides a more intuitive display of the significant positive correlation between the intensity and depth of water diffusion and enzyme activity, may be one of the reasons why the activity of F182T is slightly higher than the wild type but still significantly different from F182A.

We performed enhanced sampling for mutant F182A, F182T and WT to measure the energetic effect of the F182 mutation. The potential of mean force (PMF) of three basically converged from 0.8 ns (Fig. S4F–H†). In the trajectories of these pulling simulations, H_2O_2s try to move toward the middle of the tunnel to avoid the attraction of residues under the harmonic potential. For F182A, H_2O_2 did not cause significant conformational changes to the surrounding residues and substrate because there is sufficient space for it to pass through. For F182T, H_2O_2 slightly widens the distance between T182 and D251 in order to pass through the tunnel. In contrast, H_2O_2 induces the rotation of the benzene ring of F182 to facilitate entry into the tunnel for the WT protein. This conformational change then compels the methoxyl groups on the substrate to also undergo a conformational change towards the heme (Fig. 3C). The difference in the potential barriers of these processes is well reflected in the PMF (Fig. 4A). In F182A, the potential energy difference between the starting point (1.3 nm) and the endpoint (0.45 nm) is only about 5 kcal mol^{-1}, which is entirely possible by the internal energy of

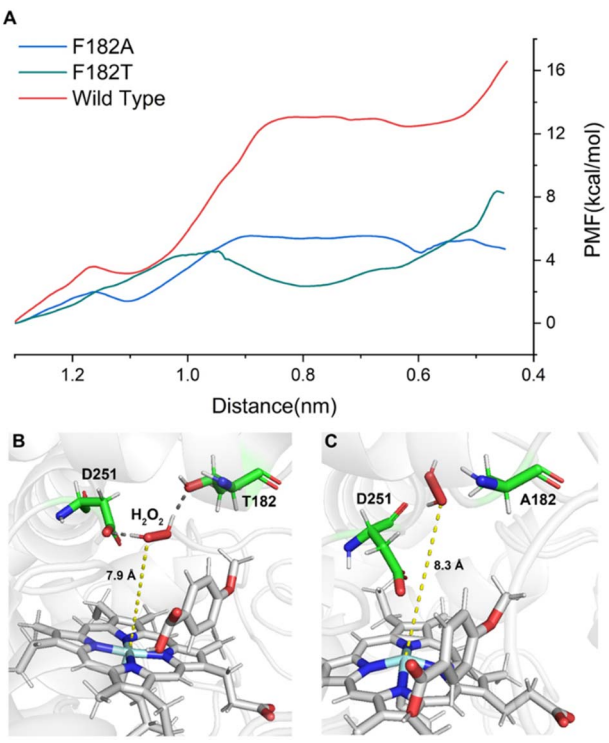

Fig. 4 (A) Comparison of the PMF for F182A, F182T and wild-type CYP199A4 (the distance between H_2O_2 and the Fe atom was set as the reaction coordinate). (B and C) Conformations around 0.8 nm between H_2O_2 and Fe in F182T and F182A, respectively.

H_2O_2 to pass through. In WT, the potential energy difference reaches ~17 kcal mol^{-1}, suggesting a significant obstruction caused by the side chain of F182 and the substrate. It is worth noting that we observed a decrease in the potential energy of F182T from less than 1 nm to a minimum at 0.8 nm (even 2–3 kcal mol^{-1} lower than F182A), followed by a gradual increase, ultimately reaching 8 kcal mol^{-1}, which is more than 3 kcal higher than F182A.

It is clear that this negative correlation between the energy barrier for H_2O_2 to traverse and enzyme activity logically aligns with the positive correlation mentioned above between the number of H_2Os and streamlines with enzyme activity. By analyzing the conformations of both around 0.8 nm, we found that in F182T, both T182 and D251 can simultaneously form hydrogen bonds with H_2O_2 (Fig. 4B). With both of them acting simultaneously, H_2O_2 can more easily reach the position parallel to them (0.8 nm). As H_2O_2 continues to penetrate, these interactions begin to hinder its progress, leading to an increase in potential energy that eventually surpasses that of F182A. In F182A, the entry of H_2O_2 is not significantly affected by interaction from the residues (Fig. 4C), resulting in a more stable potential energy. So the efficiency of H_2O_2 passing in F182T should be slightly lower than in F182A, but still much higher than in the WT. This result is consistent with the variation in the number of H_2Os inside the tunnels in their respective crystal structures, which may help to explain the differences in activity among F182A, F182T, and WT.

Catalytic *O*-demethylation of methoxy-substituted benzoic acids

A small library of engineered CYP199A4 peroxygenase variants with good to excellent catalytic activity for the demethylation of 4-MBA, including F182A, F182A/K89A, F182A/P90A, F182A/F185A, F182A/S247G, F182A/F298S and F182A/V355A, were selected to examine the scope of methoxy-substituted benzoic acids (Fig. 5), because they catalysed 4-MBA 100 times more

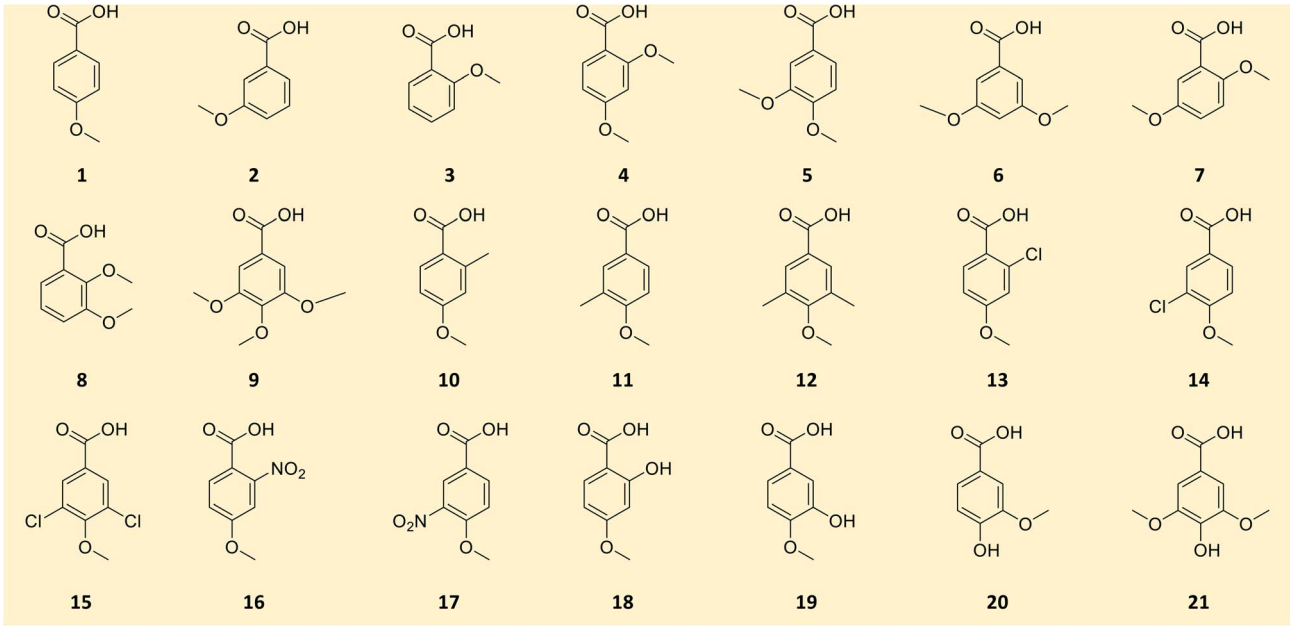

Sub	K_d (μM)	Demethylation product [a]	TON	Sub	K_d (μM)	Demethylation product [a]	TON
1	0.65	4-hydroxybenzoic acid	1100±29	**12**	123.4	not detected	-
2	29.7	3-hydroxybenzoic acid	108±2	**13**	40.1	2-chloro-4-hydroxybenzoic acid	565±10
4	69.8	2-Methoxy-4-hydroxybenzoic acid	418±19	**14**	2.0	3-chloro-4-hydroxybenzoic acid	680±13
5	13.1	3-Methoxy-4-hydroxybenzoic acid	836±19	**16**	nd	2-Nitro-4-hydroxybenzoic acid	165±7
6	10.9	3-Hydroxy-5-methoxybenzoic acid	266±1	**17**	nd	3-Nitro-4-hydroxybenzoic acid [b]	926±99
10	67.2	2-Methyl-4-hydroxybenzoic acid	645±1	**18**	1.7	2,4-dihydroxybenzoic acid	747±16
11	1.7	3-Methyl-4-hydroxybenzoic acid	1290±15	**19**	2.9	3,4-dihydroxybenzoic acid	1023±15

Fig. 5 Methoxy-substituted benzoic acid derivatives examined in this study and their dissociation constants (K_d) to the F182A mutant, as well as the catalytic TONs for the formation of the corresponding demethylation products. [a]Reaction conditions: P450 (1 μM), substrate (2 mM), 2 (10 mM) in 1 mL Tris–HCl (pH 7.4) at 30 °C. nd = not detected; TON: turnover numbers were estimated over a 60 min reaction; not detected: no demethylation products were detected; [b]the further hydroxylated product 3-nitro-4,5-dihydroxybenzoic acid (TON: 416 ± 59) from the demethylated product 3-nitro-4-hydroxybenzoic acid of **17** was also detected.

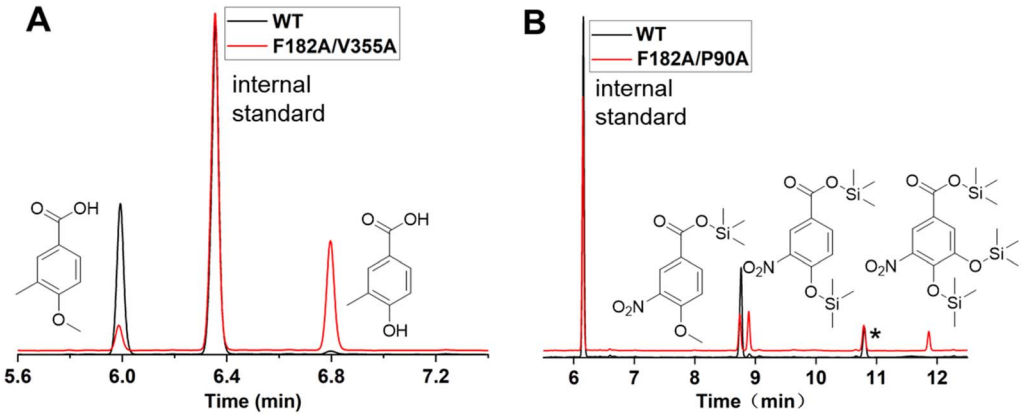

Fig. 6 Typical gas chromatographic spectra of *O*-demethylated products from substrates **11** (A) and **17** (B) catalyzed by wild-type CYP199A4, F182A/V355A, and the F182A/P90A mutant. Conditions: P450 enzyme (1 μM), substrate (2 mM), H_2O_2 (10 mM) in 1 mL Tris–HCl (pH 7.4) at 30 °C. Internal standard: benzophenone. *Impurity peak.

than the wild type. As observed in the demethylation reactions catalyzed by the NADH-dependent CYP199A4 enzymes, the examined P450 peroxygenase variants showed a good preference toward *p*-methoxy-substituted benzoic acid derivatives (Fig. 5, compounds **1**, **4**, **5**, **10–14**, **16–19**). The substrates 4-MBA with 3-substituents (either electron-donating or electron-withdrawing), such as **5**, **11**, **14** and **19**, were readily catalyzed to give the corresponding 4-demethylation products accompanied with good to excellent catalytic TONs (Fig. S6, S7, S9–S16, Tables S4, S5 and S7–S14†). The best TON of 1290 μM $(\mu M\ P450)^{-1}$ was observed for the reaction of 3-methyl-4-methoxybenzoic acid (**11**) catalyzed by the F182A/V355A mutant (Fig. 6A), which is higher than that of 4-MBA [**1**, TON = 1100 μM $(\mu M\ P450)^{-1}$] by F182A/P90A. Noteworthy, the oxidation of 4-methoxy-3-nitrobenzoic acid (**17**) by F182A/P90A yielded demethylated 4-hydroxy-3-nitrobenzoic acid and the over-oxidation product 4,5-dihydroxy-3-nitrobenzoic acid with TONs of 926 and 416 μM $(\mu M\ P450)^{-1}$, respectively (Fig. 6B). This is an interesting result because no 2-hydroxylation of benzoic acid derivatives by CYP199A4 enzymes has been observed previously. P90 is an amino acid at the entrance of the substrate channel and is located on the surface of CYP199A4; mutating it to A not only increases the diameter of the entrance of the substrate channel and accelerates the rate of substrate entry, but also allows a small amount of H_2O_2 to enter the haematoxylin active centre of CYP199A4 through the substrate channel, which in turn improves the *O*-demethylation capacity of F182A/P90A. Similarly, V355 is located on the surface of CYP199A4 and is a key amino acid residue at the entrance of the tunnel, and mutating it to alanine increased the diameter of this tunnel, allowing more H_2O_2 to enter the active pocket of CYP199A4 and increasing the peroxidase activity of F182A/V355A. In addition, either 3-methoxybenzoic acid (**2**) or 3,5-dimethoxybenzoic acid (**6**) can be demethylated to produce 3-hydroxylation phenols (Fig. S5, S8, Tables S3 and S6†). In contrast, Bell *et al.* found that the monooxygenase CYP199A4 was not able to catalyse the *O*-demethylation reaction of benzoic acid substituted with methoxy at the 3-position.[27–29] However, both 2,5-dimethoxybenzoic acid (**7**) and 2,3-dimethoxybenzoic acid (**8**) are not converted by the CYP199A4 variants, suggesting that the substituent at the 2-position may be unfavorable. Moreover, no reaction product was detected from the oxidation of 2-methoxybenzoic acid (**3**) by the examined enzymes. All 4-methoxybenzoid acids with 2-substituents (**4**, **10**, **13**, **16**, **18**) showed lower catalytic TONs than those with identical substituents at the 3-position (**5**, **11**, **14**, **17**, **19**). Although substrate **19** has a guaiacol structural unit, unfortunately, substrate 4-hydroxy-3-methoxybenzoic acid (**20**), a more approximate H-type lignin monomer, was not demethylated by the variants. Similarly, the variants did not convert the S-type lignin monomer analog, 4-hydroxy-3,5-dimethoxybenzoic acid (**21**). In addition, there were no conversions detected for substrates with large steric hindrance substituents at positions 3 and 5 of the benzene ring, such as 3,4,5-trimethoxy benzoic acid (**9**) and 3,5-dichloro-4-methoxy benzoic acid (**15**). However, substrates with a smaller steric hindrance, such as 3,5-dimethyl-4-methoxy benzoic acid (**12**), were catalyzed by the mutant F182A/V355A to yield a single product (not 3,5-dimethyl-4-hydroxybenzoic acid) (Fig. S17†).

Finally, the milligram scale reaction of 3-methyl-4-methoxybenzoic acid was validated using F182A/V355A (4 μM) in 50 mL 50 mM Tris–HCl (pH 7.4) in the presence of 10 mM H_2O_2 at 30 °C for 10 min. As a result, 3-methyl-4-hydroxybenzoic acid was isolated as a powder (18.0 mg, 59%) (Fig. S18†), indicating that this system has great potential for applications.

Binding affinity of substrates

The K_d values of mutant F182A toward each substrate were determined using UV-visible spectral titration experiments to analyze the binding of the substrates (Fig. 5 and S19–S30†). The binding affinity of substrates shows a specific positive correlation with the catalytic activity of the CYP199A4 mutants. 3-Methyl-4-methoxybenzoic acid (**11**) showed the optimal *O*-demethylation activity and considerable binding affinity to F182A (K_d = 1.7 μM), whereas 4-MBA (**1**) showed the strongest binding affinity to F182A (K_d = 0.65 μM) together with high

catalytic activity. Similarly, the strong affinity of the protein toward specific substrates (*e.g.*, **5**, **14**, **18**, **19**) also gave considerable catalytic activity. In contrast, substrates **3**, **7**–**9**, **15**, **20** and **21** did not show any *O*-demethylation activity and measuring the K_d values was not possible. In addition, although 3,5-dimethyl-4-methoxybenzoic acid (**12**) showed weak binding to F182A (K_d = 123.4 μM), no corresponding demethylation product was detected. The K_d values of 2-nitro-4-methoxybenzoic acid (**16**) and 3-nitro-4-methoxybenzoic acid (**17**) were not determined because of the close UV absorption region of the nitro group with the iron heme.

Conclusions

We have combined X-ray crystallography and MD simulations to disclose the crucial gating role of F182 and D251 in regulating H_2O inflow into the active site of CYP199A4, thereby providing a mechanistic understanding to generate or enhance peroxygenase activity of CYP199A4 by engineering an H_2O_2 tunnel. In general, the mechanism indicates the feasibility of the HTE strategy to convert NAD(P)H-dependent P450 monooxygenases into their peroxygenase modes. The CYP199A4 peroxygenase variants engineered using this strategy showed moderate to excellent catalytic activity toward *O*-demethylation of methoxy-substituted benzoic acid derivatives. Preferential binding of *para*- and *meta*-position substrates indicates the potential of engineering CYP199A4 for converting lignin monomers. This study provides insights into developing non-native P450 peroxygenases for valuable organic transformations.

Data availability

All experimental data and detailed experimental procedures are available in the published article and ESI.†

Author contributions

Z. C. conceptualization, supervision, project administration, and resources; P. Z., Y. J., and Q. W. data curation, formal analysis, investigation, methodology, and writing – original draft; Z. C., Y. J., and J. C. funding acquisition; J. C. and F. Y. validation; Z. C., P. Z., Y. J., and Q. W. writing – review & edition.

Conflicts of interest

The authors declare no conflict of interest.

Acknowledgements

This work was supported by the National Key Research and Development Program of China (2023YFA0915500 to Z. C.), National Natural Science Foundation of China (32371311 to Z. C.; 22207112 to Y. J.; 22107105 to J. C.), and QIBEBT/SEI/QNESL (S202302 to Z. C.). We thank the staff of BL19U1 beamlines at the Shanghai Synchrotron Radiation Facility for assistance during X-ray diffraction data collection. We thank Liwen Bianji (Edanz) for editing the English text of a draft of this manuscript.

Notes and references

1 R. Saini, A. Kaur, J. K. Saini, A. K. Patel, S. Varjani, C.-W. Chen, R. R. Singhania and C.-D. Dong, *BioEnergy Res.*, 2022, **16**, 88–104.
2 Z.-H. Liu, R. K. Le, M. Kosa, B. Yang, J. Yuan and A. J. Ragauskas, *Renew. Sustain. Energy Rev.*, 2019, **105**, 349–362.
3 G. Fuchs, M. Boll and J. Heider, *Nat. Rev. Microbiol.*, 2011, **9**, 803–816.
4 T. Abe, E. Masai, K. Miyauchi, Y. Katayama and M. Fukuda, *J. Bacteriol.*, 2005, **187**, 2030–2037.
5 E. Masai, M. Sasaki, Y. Minakawa, T. Abe, T. Sonoki, K. Miyauchi, Y. Katayama and M. Fukuda, *J. Bacteriol.*, 2004, **186**, 2757–2765.
6 S. J. B. Mallinson, M. M. Machovina, R. L. Silveira, M. Garcia-Borras, N. Gallup, C. W. Johnson, M. D. Allen, M. S. Skaf, M. F. Crowley, E. L. Neidle, K. N. Houk, G. T. Beckham, J. L. DuBois and J. E. McGeehan, *Nat. Commun.*, 2018, **9**, 2487.
7 M. Nishimura, Y. Nishimura, C. Abe and M. Kohhata, *Biol. Pharm. Bull.*, 2014, **37**(9), 1564–1568.
8 R. Bernhardt and V. B. Urlacher, *Appl. Microbiol. Biotechnol.*, 2014, **98**, 6185–6203.
9 M. M. Fetherolf, D. J. Levy-Booth, L. E. Navas, J. Liu, J. C. Grigg, A. Wilson, R. Katahira, G. T. Beckham, W. W. Mohn and L. D. Eltis, *Proc. Natl. Acad. Sci. U. S. A.*, 2020, **117**, 25771–25778.
10 S. G. Bell, A. B. Tan, E. O. Johnson and L. L. Wong, *Mol. BioSyst.*, 2010, **6**, 206–214.
11 N. Ma, Z. Chen, J. Chen, J. Chen, C. Wang, H. Zhou, L. Yao, O. Shoji, Y. Watanabe and Z. Cong, *Angew. Chem., Int. Ed.*, 2018, **57**, 7628–7633.
12 H. Joo, Z. Lin and F. H. Arnold, *Nature*, 1999, **399**(6737), 670–673.
13 P. C. Cirino and F. H. Arnold, *Angew. Chem., Int. Ed.*, 2003, **42**, 3299–3301.
14 Y. Jiang, C. Wang, N. Ma, J. Chen, C. Liu, F. Wang, J. Xu and Z. Cong, *Catal. Sci. Technol.*, 2020, **10**, 1219–1223.
15 M. N. Podgorski, J. S. Harbort, J. H. Z. Lee, G. T. H. Nguyen, J. B. Bruning, W. A. Donald, P. V. Bernhardt, J. R. Harmer and S. G. Bell, *ACS Catal.*, 2022, **12**, 1614–1625.
16 M. N. Podgorski, T. Coleman, L. R. Churchman, J. B. Bruning, J. J. De Voss and S. G. Bell, *Chem.–Eur. J.*, 2022, **28**, e202202428.
17 A. C. Harlington, K. E. Shearwin, S. G. Bell and F. Whelan, *Chem. Commun.*, 2022, **58**, 13321–13324.
18 P. Zhao, F. Kong, Y. Jiang, X. Qin, X. Tian and Z. Cong, *J. Am. Chem. Soc.*, 2023, **145**, 5506–5511.
19 S. G. Bell, W. Yang, A. B. Tan, R. Zhou, E. O. Johnson, A. Zhang, W. Zhou, Z. Rao and L. L. Wong, *Dalton Trans.*, 2012, **41**, 8703–8714.
20 G. P. Bienert and F. Chaumont, *Biochim. Biophys. Acta*, 2014, **1840**, 1596–1604.
21 T. Henzler and E. Steudle, *J. Exp. Bot.*, 2000, **51**(353), 2053–2066.

22 T. L. Poulos, *Chem. Rev.*, 2014, **114**, 3919–3962.
23 P. Vidossich, G. Fiorin, M. Alfonso-Prieto, E. Derat, S. Shaik and C. Rovira, *J. Phys. Chem. B*, 2010, **114**(15), 5161–5169.
24 S. Vassiliev, T. Zaraiskaya and D. Bruce, *Biochim. Biophys. Acta*, 2012, **1817**, 1671–1678.
25 S. Vassiliev, P. Comte, A. Mahboob and D. Bruce, *Biochemistry*, 2010, **49**, 1873–1881.
26 C. Gustafsson, S. Vassiliev, C. Kurten, P. O. Syren and T. Brinck, *ACS Omega*, 2017, **2**, 8495–8506.
27 M. N. Podgorski, T. Coleman, R. R. Chao, J. J. De Voss, J. B. Bruning and S. G. Bell, *J. Inorg. Biochem.*, 2020, **203**, 110913.
28 T. Coleman, R. R. Chao, J. B. Bruning, J. J. De Voss and S. G. Bell, *RSC Adv.*, 2015, **5**, 52007–52018.
29 T. Coleman, S. H. Wong, M. N. Podgorski, J. B. Bruning, J. J. De Voss and S. G. Bell, *ACS Catal.*, 2018, **8**, 5915–5927.